

MIT Open Access Articles

Polaron effects on the performance of light-harvesting systems: a quantum heat engine perspective

The MIT Faculty has made this article openly available. **Please share** how this access benefits you. Your story matters.

Citation: Xu, Dazhi et al. "Polaron Effects on the Performance of Light-Harvesting Systems: A Quantum Heat Engine Perspective." *New Journal of Physics* 18.2 (2016): 023003. © 2016 IOP Publishing Ltd and Deutsche Physikalische Gesellschaft

As Published: <http://dx.doi.org/10.1088/1367-2630/18/2/023003>

Publisher: IOP Publishing

Persistent URL: <http://hdl.handle.net/1721.1/108522>

Version: Final published version: final published article, as it appeared in a journal, conference proceedings, or other formally published context

Terms of use: Creative Commons Attribution



Polaron effects on the performance of light-harvesting systems: a quantum heat engine perspective

This content has been downloaded from IOPscience. Please scroll down to see the full text.

2016 New J. Phys. 18 023003

(<http://iopscience.iop.org/1367-2630/18/2/023003>)

View [the table of contents for this issue](#), or go to the [journal homepage](#) for more

Download details:

IP Address: 18.51.1.3

This content was downloaded on 09/05/2016 at 19:06

Please note that [terms and conditions apply](#).



PAPER

OPEN ACCESS

RECEIVED

17 September 2015

REVISED

13 December 2015

ACCEPTED FOR PUBLICATION

17 December 2015

PUBLISHED

28 January 2016

Original content from this work may be used under the terms of the [Creative Commons Attribution 3.0 licence](#).

Any further distribution of this work must maintain attribution to the author(s) and the title of the work, journal citation and DOI.



Polaron effects on the performance of light-harvesting systems: a quantum heat engine perspective

Dazhi Xu^{1,2}, Chen Wang^{2,3}, Yang Zhao¹ and Jianshu Cao^{2,4}¹ School of Materials Science and Engineering, Nanyang Technological University, Singapore² Department of Chemistry, Massachusetts Institute of Technology, Cambridge, MA 02139, USA³ Department of Physics, Hangzhou Dianzi University, Hangzhou, Zhejiang 310018, People's Republic of China⁴ Singapore-MIT Alliance for Research and Technology, 1 CREATE Way, Singapore 138602, SingaporeE-mail: jianshu@mit.edu**Keywords:** quantum open system, heat engine, strong coupling

Abstract

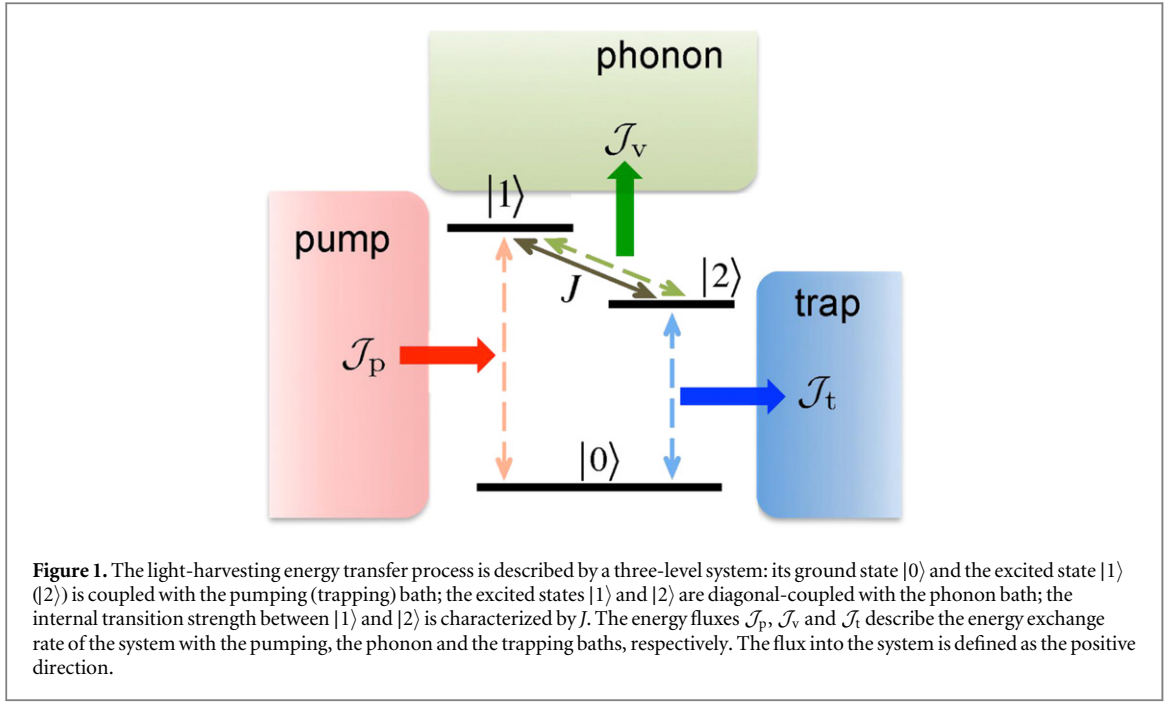
We explore energy transfer in a generic three-level system, which is coupled to three non-equilibrium baths. Built on the concept of quantum heat engine, our three-level model describes non-equilibrium quantum processes including light-harvesting energy transfer, nano-scale heat transfer, photo-induced isomerization, and photovoltaics in double quantum-dots. In the context of light-harvesting, the excitation energy is first pumped up by sunlight, then is transferred via two excited states which are coupled to a phonon bath, and finally decays to the reaction center. The efficiency of this process is evaluated by steady state analysis via a polaron-transformed master equation; thus the entire range of the system-phonon coupling strength can be covered. We show that the coupling with the phonon bath not only modifies the steady state, resulting in population inversion, but also introduces a finite steady state coherence which optimizes the energy transfer flux and efficiency. In the strong coupling limit, the steady state coherence disappears and the efficiency recovers the heat engine limit given by Scovil and Schultz-Dubois (1959 *Phys. Rev. Lett.* **2** 262).

1. Introduction

With the rapid developments in measurement and manipulation of microscopic systems, quantum effects such as coherence and entanglement are often utilized to enhance the performance of microscopic devices. Even in biological systems, both experiments [1] and theoretical models [2, 3] reveal that the long-lived quantum coherence may play an important role in highly efficient energy and electron transfer processes. How biological systems, such as light-harvesting complex, preserve such long-lived coherence and how nature benefits from the coherence are two key questions that define the emerging field of quantum biology.

Taking a three-level system as a generic theoretical model, many interesting mechanisms can be well demonstrated and understood. Recently, the sunlight-induced exciton coherence is studied in a V-configuration three-level model [4, 5]. An interesting idea is to consider the energy transfer process from the perspective of heat engine [6]. For example, the coherence introduced by an auxiliary energy level can enhance the heat engine power [7, 8]. The early work considering a three-level maser model as a Carnot engine was carried out by Scovil and Schulz-DuBois [9, 10], yielding the heat engine efficiency η_0 and its relation with the Carnot efficiency. Later papers elaborately reexamined the dynamics of this model by the Lindblad master equation and showed that the thermodynamic efficiency η_0 is achieved when the output light-field is strongly coupled with the three-level system [11–13]. The quantum heat engine provides us a heuristic perspective to better understand the basic physical processes in energy transfer and presents useful insight to enhance the efficiency and output power in small systems [14–17].

In this paper, we study the polaron effects of a phonon bath on the energy transfer flux and efficiency in a generic three-level model. The energy transfer efficiency is defined as the ratio between the trapping and pumping fluxes. The canonical distribution of a thermal equilibrium system requires a negligible coupling



between the system and its environment. As the coupling strength grows, the steady state of the system will no longer be canonical [18–22]. This non-canonical state actually introduces the steady state coherence into the system without refereeing to specific forms of light–matter interaction or designing exotic system configurations. The bath-induced coherent effect is investigated by the polaron-transformed Redfield equation (PTRE) [23, 24], which bridges both the weak and strong system–bath coupling regions. The difference between the steady state efficiency and strong coupling limit η_0 depends strongly on the phonon-induced coherence. Taking into account of the behavior of both the flux and efficiency, we are able to optimize coupling and temperature in designing optimal artificial energy transfer systems.

In this paper, we first introduce the three-level model and its non-equilibrium environment in section 2, and then formulate the PTRE in section 3. In section 4, the polaron effects of phonon-bath on the energy transfer flux and efficiency are studied in detail. We summarize our results in the last section. We leave the detailed derivation and properties of the PTRE in the appendix.

2. Three-level system model

2.1. Model system

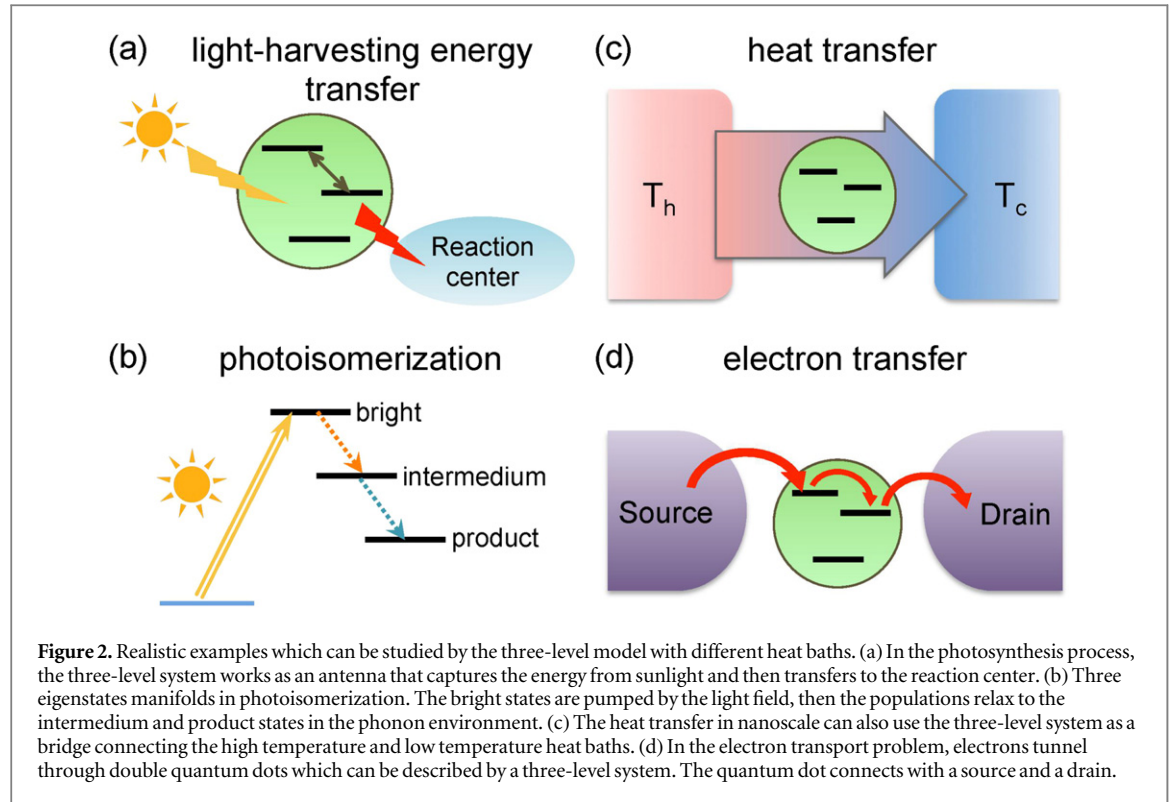
We consider the energy transfer process in the three-level system illustrated in figure 1. The site energy of the ground state $|0\rangle$ is set to zero. The two excited energy levels $|1\rangle$ and $|2\rangle$ form a two-level system (TLS, in the following the TLS is referred to the two excited states), with the corresponding site energy ϵ_1 and ϵ_2 . The transition due to the dipole–dipole interaction is characterized by J . Then the three-level system is modeled by the Hamiltonian H_0 as:

$$H_0 = \sum_{i=1,2} \epsilon_i |i\rangle \langle i| + \frac{J}{2} (|1\rangle \langle 2| + |2\rangle \langle 1|). \quad (1)$$

We are interested in the transfer process in the single excitation subspace: the three-level system is firstly excited to state $|1\rangle$ by a photon field, then the excitation is transferred to state $|2\rangle$ through J (mediated by phonon modes), and finally the excitation decays to the ground state $|0\rangle$ via spontaneous radiation. The pumping and trapping processes are modeled by the interaction with the two independent photon baths, which are coupled separately with two transitions $|0\rangle \leftrightarrow |1\rangle$ and $|0\rangle \leftrightarrow |2\rangle$. The Hamiltonian of the photon baths and their interactions with the three-level system are given by

$$H_p = \sum_k \omega_{pk} a_{pk}^\dagger a_{pk} + (g_{pk} a_{pk}^\dagger |0\rangle \langle 1| + \text{h.c.}), \quad (2)$$

$$H_t = \sum_k \omega_{tk} a_{tk}^\dagger a_{tk} + (g_{tk} a_{tk}^\dagger |0\rangle \langle 2| + \text{h.c.}), \quad (3)$$



where ω_{ik} ($i = p, t$) is the eigen frequency of the bath mode described by the creation (annihilation) operator a_{ik}^\dagger (a_{ik}), and its coupling strength to the excited state is g_{ik} . We note that the rotating wave approximation is applied in the system–bath interaction term. A phonon bath with creation and annihilation operators b_k^\dagger and b_k of the bath mode ω_{vk} is coupled to the TLS via diagonal interaction with the coupling strength of f_k . Thus, the phonon part is described by

$$H_v = \sum_k \omega_{vk} b_k^\dagger b_k + (|1\rangle\langle 1| - |2\rangle\langle 2|) \sum_k (f_k b_k^\dagger + \text{h.c.}). \quad (4)$$

This microscopic three-level system immersed in the non-equilibrium environment was studied as a quantum heat pump phenomenologically without considering the details of the system–bath coupling [10]. In the case that the phonon bath is replaced by a single driving mode strongly coupled to the system, the dynamic steady states have been solved and the efficiency is given by $\eta_0 = \epsilon_2/\epsilon_1$ [12, 13]. In reality, the three-level model can be realized in both nature and laboratory. Taking the energy transfer process in photosynthetic pigment for example (figure 2(a)), different baths could arise from different sources: the pumping light field (such as the sunlight photons) is considered as a high temperature boson bath; the trapping bath is formed by the surrounding electromagnetic environment which models the energy transfer to the reaction center; and the phonon bath with inverse temperature β_v describes the phonon modes coupled with the excited states. In addition, such a three-level (or more intermediate energy levels) system is used to describe photoisomerization (figure 2(b)), nanoscale heat transfer [25] (figure 2(c)) or photovoltaic current in double quantum dots [26] (figure 2(d)).

In this paper, we focus on the effects of the phonon modes on energy flux and efficiency. Usually when the system–phonon bath coupling strength is not weak, the Bloch–Redfield equation approach cannot be applied. Therefore, we will introduce the PTRE [23, 24], which gives reliable results from the weak to strong coupling region using super Ohmic bath spectrum with large cut-off frequency ω_c , to study the bath-induced coherent effects of this quantum system. The validity of the PTRE has been verified by comparing with the numerical path integral method [21] and time-convolutionless polaron master equation [27, 28].

2.2. Definitions of energy flux and transfer efficiency

We are interested in the energy transfer flux and efficiency of the three-level system at its non-equilibrium steady state. The steady state solution can be obtained by the master equation formally written as

$$\frac{d\rho(t)}{dt} = (\mathcal{L}_0 + \mathcal{L}_p + \mathcal{L}_v + \mathcal{L}_t)\rho(t), \quad (5)$$

which describes the dynamics of the reduced density matrix (RDM) $\rho(t)$ of the three-level system. The Liouville operator \mathcal{L}_0 denotes the non-dissipative term, \mathcal{L}_p , \mathcal{L}_v and \mathcal{L}_t denote the dissipation effects associated with the pumping, phonon coupling, and trapping, respectively.

To quantitatively investigate the energy transfer process, we define the steady state energy fluxes by calculating the energy change of the three-level system

$$\begin{aligned}\dot{E}(\infty) &= \text{Tr}_s \left[\frac{d\rho(t)}{dt} H_0 \right]_{t=\infty} = \sum_{i=p,v,t} \text{Tr}_s [\mathcal{L}_i[\rho(\infty)] H_0] \\ &\equiv \mathcal{J}_p + \mathcal{J}_v + \mathcal{J}_t.\end{aligned}\quad (6)$$

It can be shown that $\text{Tr}_s[\mathcal{L}_0 H_0] = 0$. The three energy fluxes \mathcal{J}_i , $i = p, v, t$ are defined with respect to their corresponding dissipation operator \mathcal{L}_i . These energy fluxes have clear physical meanings of the energy exchange rate with the pumping field, phonon environment, and trapping field, respectively. In this work, we are interested in the steady state, in equation (6) the fluxes are calculated with $\rho(\infty)$, which is obtained by solving $\dot{\rho}(t) = 0$. Straightforwardly, we define the energy transfer efficiency by

$$\eta = \left| \frac{\mathcal{J}_t(\infty)}{\mathcal{J}_p(\infty)} \right|, \quad (7)$$

which is the ratio between the output and the input energy fluxes.

Without losing generality, we assume the pumping (trapping) bath is weakly coupled with the system and can be described phenomenologically by the local Liouville operator of the Lindblad form

$$\begin{aligned}\mathcal{L}_i[\rho] &= \frac{\gamma_i}{2} [(n_i + 1)(2O_i^- \rho O_i^+ - \{O_i^+ O_i^-, \rho\}) \\ &\quad + n_i(2O_i^+ \rho O_i^- - \{O_i^- O_i^+, \rho\})],\end{aligned}\quad (8)$$

where $i = p, t$ refers to the two photon baths, γ_i and n_i are the corresponding decay rate and average photon number, and the system operators are defined as $O_p^+ = |1\rangle\langle 0|$, $O_t^+ = |2\rangle\langle 0|$. The system-phonon bath coupling will be treated more rigorously as we are interested in how this coupling affects the energy transfer over a broad range. To achieve this goal, we apply the PTRE equation, which will be introduced in the following section.

3. PTRE

The Redfield master equation is valid up to the second-order perturbation of the system-bath interaction. In order to go beyond this weak coupling limit, polaron transformation is introduced to incorporate the high-order system-bath interaction into the dynamics of the system. Here we focus on the coupling strength between the system and phonon bath, and the polaron transformation is only related to the two excited states. Therefore it is convenient to consider the TLS first, then the resulting Liouville operator describing the TLS dissipative process can be incorporated into the dynamics of the three-level system.

We employ the Pauli matrix $\sigma_x = |1\rangle\langle 2| + |2\rangle\langle 1|$ and $\sigma_z = |1\rangle\langle 1| - |2\rangle\langle 2|$, and define the polaron transformation

$$\tilde{H}' = e^{-i\sigma_z B/2} H' e^{i\sigma_z B/2} = \tilde{H}_0 + \tilde{H}_b + \tilde{V}, \quad (9)$$

where $H' = H_0 + H_v$ is the Hamiltonian of the TLS with the phonon bath, the collective bath operator is $B = 2i \sum_k (f_k b_k^\dagger - f_k^* b_k) / \omega_{vk}$ and

$$\tilde{H}_0 = \frac{\epsilon}{2} \sigma_z + \frac{J}{2} \kappa \sigma_x, \quad (10)$$

$$\tilde{H}_b = \sum_k \omega_{vk} b_k^\dagger b_k - \sum_k \frac{|f_k|^2}{\omega_{vk}}, \quad (11)$$

$$\tilde{V} = \frac{J}{2} [\sigma_x (\cos B - \kappa) + \sigma_y \sin B]. \quad (12)$$

The transformed system-bath interaction is \tilde{V} and $\epsilon = \epsilon_1 - \epsilon_2$. The expectation value of the bath operator

$$\begin{aligned}\kappa &= \text{Tr}_b [\rho_b' \cos B] \\ &= \exp \left[- \int_0^\infty d\omega \frac{J(\omega)}{\pi \omega^2} \left(n_v(\omega) + \frac{1}{2} \right) \right]\end{aligned}\quad (13)$$

is subtracted from \tilde{V} as a renormalization factor, with $\rho_b' = \exp(-\beta_v \tilde{H}_b) / \text{Tr}_b [\exp(-\beta_v \tilde{H}_b)]$ the thermal state of the phonon bath and $n_v(\omega) = [\exp(\beta_v \omega) - 1]^{-1}$ the average phonon number. The spectrum function is

chosen to be super-Ohmic as

$$J(\omega) = 4\pi \sum_k |f_k|^2 \delta(\omega - \omega_k) = \alpha \pi \omega^3 \omega_c^{-2} e^{-\omega/\omega_c}, \quad (14)$$

where ω_c is the cut-off frequency and α is a dimensionless parameter characterizing the system–bath coupling which is proportional to λ/ω_c (λ is the reorganization energy). It can be verified that the thermal average of \tilde{V} is zero, i.e., \tilde{V} is of the order of bath fluctuations and thus is a reliable perturbation parameter. Based on this consideration, the Born–Markov approximation is applied to derive the PTRE in the Schrodinger picture as

$$\begin{aligned} \frac{d\rho'_s(t)}{dt} = & -i[\tilde{H}_0, \rho'_s(t)] - \sum_{ij=z,\pm} [\Gamma_{ij}^+ \tau_i \tau_j \rho'_s(t) + \Gamma_{ji}^- \rho'_s(t) \tau_j \tau_i \\ & - \Gamma_{ji}^- \tau_i \rho'_s(t) \tau_j - \Gamma_{ij}^+ \tau_j \rho'_s(t) \tau_i]. \end{aligned} \quad (15)$$

Here, Γ_{ij}^\pm is defined by the bath correlation function. We denote ρ'_s (ρ_s) as the RDM of the TLS in the polaron (local) frame, and define a new set of Pauli operator

$$\tau_z = |+\rangle\langle+| - |-\rangle\langle-|, \quad (16)$$

$$\tau_+ = |+\rangle\langle-|, \tau_- = |-\rangle\langle+|, \quad (17)$$

where $\tilde{H}_0 |\pm\rangle = \epsilon_\pm |\pm\rangle$. The detailed derivation of the PTRE can be found in appendix A.

The PTRE was firstly introduced by Silbey and coworkers [23, 24], and has been widely used in solving the strong system–bath coupling problems. The validity of the PTRE in the whole range of coupling strength requires the bath cut-off frequency should be much larger than the internal coupling strength, $\omega_c \gg J$; if $\omega_c \lesssim J$, the PTRE only works well in the strong coupling regime [21]. To extend the valid regime of the polaron approach even for small ω_c , a variational polaron transformation can be applied, where f_k in the bath operator B is substituted with a variational parameter [21, 24, 29]. Moreover, it will be shown in B that the results given by PTRE are consistent with those given by the Redfield equation in the weak coupling limit and the Fermi's golden rule (or Frster theory) in the strong coupling limit [21, 25, 26]. Therefore, the PTRE smoothly connects the two limits, and provides a useful tool to study the intermediate coupling region where there are usually no reliable approximation methods.

For further discussion on the property of the entire three-level system with the other two weakly coupled photon baths, equation (15) for the two excited states is transformed back into the local basis and rewritten as $[\dot{\rho}'_s(t)]_{ij} = \sum_{mn} [\mathcal{L}_v]_{(ij, mn)} [\rho'_s(t)]_{mn}$. Then the expressions for the Liouville operator \mathcal{L}_v are obtained accordingly. The relations between the elements of $\rho'_s(t)$ and $\rho_s(t)$ are also given in appendix A.

The Bloch-form equation of the three-level system is derived following from equation (5). One thing should be noted, the population conservation of the TLS gives $[\rho_s(t)]_{11} + [\rho_s(t)]_{22} = 1$; while for the three-level system, the ground state population should be included and population conservation becomes $\rho_{00}(t) + \rho_{11}(t) + \rho_{22}(t) = 1$, where we denote $\rho_{ij}(t) = \langle i | \rho(t) | j \rangle$. The Liouville operator \mathcal{L}_v which considers the polaron effects has been obtained from the PTRE of the TLS. The effects of the pumping and trapping baths are described by the Lindblad operator \mathcal{L}_p and \mathcal{L}_t defined in equation (8). Therefore, the PTRE for the three-level system is given as

$$\frac{d}{dt} \begin{pmatrix} \rho_{11}(t) - \rho_{22}(t) \\ \rho_{11}(t) + \rho_{22}(t) \\ \Re[\rho_{12}(t)] \\ \Im[\rho_{12}(t)] \end{pmatrix} = -\tilde{M} \begin{pmatrix} \rho_{11}(t) - \rho_{22}(t) \\ \rho_{11}(t) + \rho_{22}(t) \\ \Re[\rho_{12}(t)] \\ \Im[\rho_{12}(t)] \end{pmatrix} + \frac{J^2}{4} \begin{pmatrix} \gamma_p n_p - \gamma_t n_t \\ \gamma_p n_p + \gamma_t n_t \\ 0 \\ 0 \end{pmatrix}, \quad (18)$$

where the matrix \tilde{M} is shown in appendix B. The equations for the off-diagonal terms $\rho_{01}(t)$ and $\rho_{02}(t)$ are decoupled from equation (18) and not related with the energy flux and transfer efficiency, thus will not involve in the following discussion.

4. Energy transfer flux and efficiency

4.1. Steady state flux

The steady state of the three-level system can be easily obtained from equation (18), which incorporates the polaron effects of the phonon bath. Then the steady state energy fluxes defined in equation (6) are straightforwardly given as

$$\mathcal{J}_p = \epsilon_1 \gamma_p [n_p \rho_{00} - (n_p + 1) \rho_{11}] - \frac{J \gamma_p}{2} (n_p + 1) \Re[\rho_{12}], \quad (19)$$

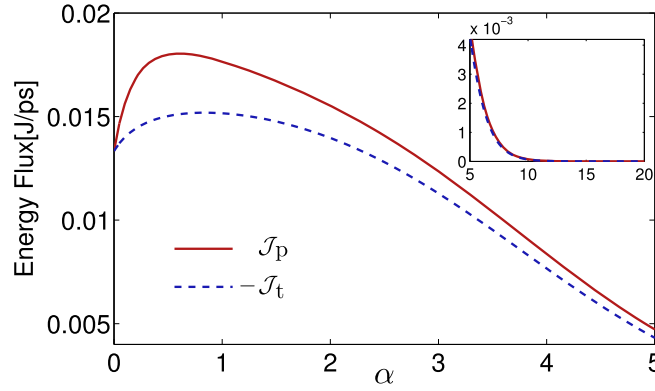


Figure 3. The steady state pumping (red solid line) and trapping (blue dashed line) energy fluxes versus α . The minus sign in front of the trapping flux suggests the energy flows into the trapping bath. Both fluxes show a maximal value in the weak coupling case and then quickly decreases to zero when α increases. The inset shows the strong coupling case. We choose the parameters in units of J : $\epsilon_1/J = 5$, $\epsilon_2/J = 4.5$, $\omega_c/J = 5$, $\beta_p J = 0.02$, $\beta_t J = \beta_v J = 1$, and $\gamma_p/J = \gamma_t/J = 0.01$.

$$\mathcal{J}_t = \epsilon_2 \gamma_t [n_t \rho_{00} - (n_t + 1) \rho_{22}] - \frac{J \gamma_t}{2} (n_t + 1) \Re[\rho_{12}], \quad (20)$$

where we denote the steady state elements of RDM by $\rho_{ij} = \langle i | \rho_s(\infty) | j \rangle$ for brevity. Figure 3 presents energy fluxes with respect to α . In the extreme case that the system bath coupling is switched off ($\alpha = 0$), there is no loss of excitation energy, which results in $\mathcal{J}_p = -\mathcal{J}_t$, suggesting the input energy flux from the pump completely flows into the trap through the three-level system (note that we chose the positive direction as that the flux flows into the system). When the coupling turns on, a portion of energy flux leaks into the phonon bath thus $\mathcal{J}_p > -\mathcal{J}_t$. Both the pumping and trapping energy fluxes reach their optimal values in the intermediate coupling region and decrease to zero when the coupling strength is strong.

In the context of heat engine, the trapping energy flux \mathcal{J}_t in our model corresponds to the output power and \mathcal{J}_p corresponds to the input power. Usually, the power of a heat engine is small when the efficiency is high. Particularly, at the maximal efficiency, all the processes are required to be quasi-static and take infinite time, and thus the power will be zero. To balance the conflict between the efficiency and power, much work has been done to study the efficiency at maximum power [30–32]. In the following, we will calculate the energy transfer efficiency of our system and show its competitive relation with the trapping flux, in analogy to the efficiency and power in the heat engine.

4.2. Steady state efficiency

Before presenting the result of efficiency defined in equation (7), we begin with the analysis of the limiting cases. The first term on the right side of equations (19) and (20) depends only on the populations of the three-level system, and the second term represents the contribution of the off-diagonal terms (coherence in the local basis). As we show in figure C1 of appendix C, the steady state coherence in the local bases ρ_{12} vanishes in the strong coupling limit, then the efficiency is completely determined by the populations. According to the steady state solution of the second equation in equation (18), we obtain the relation

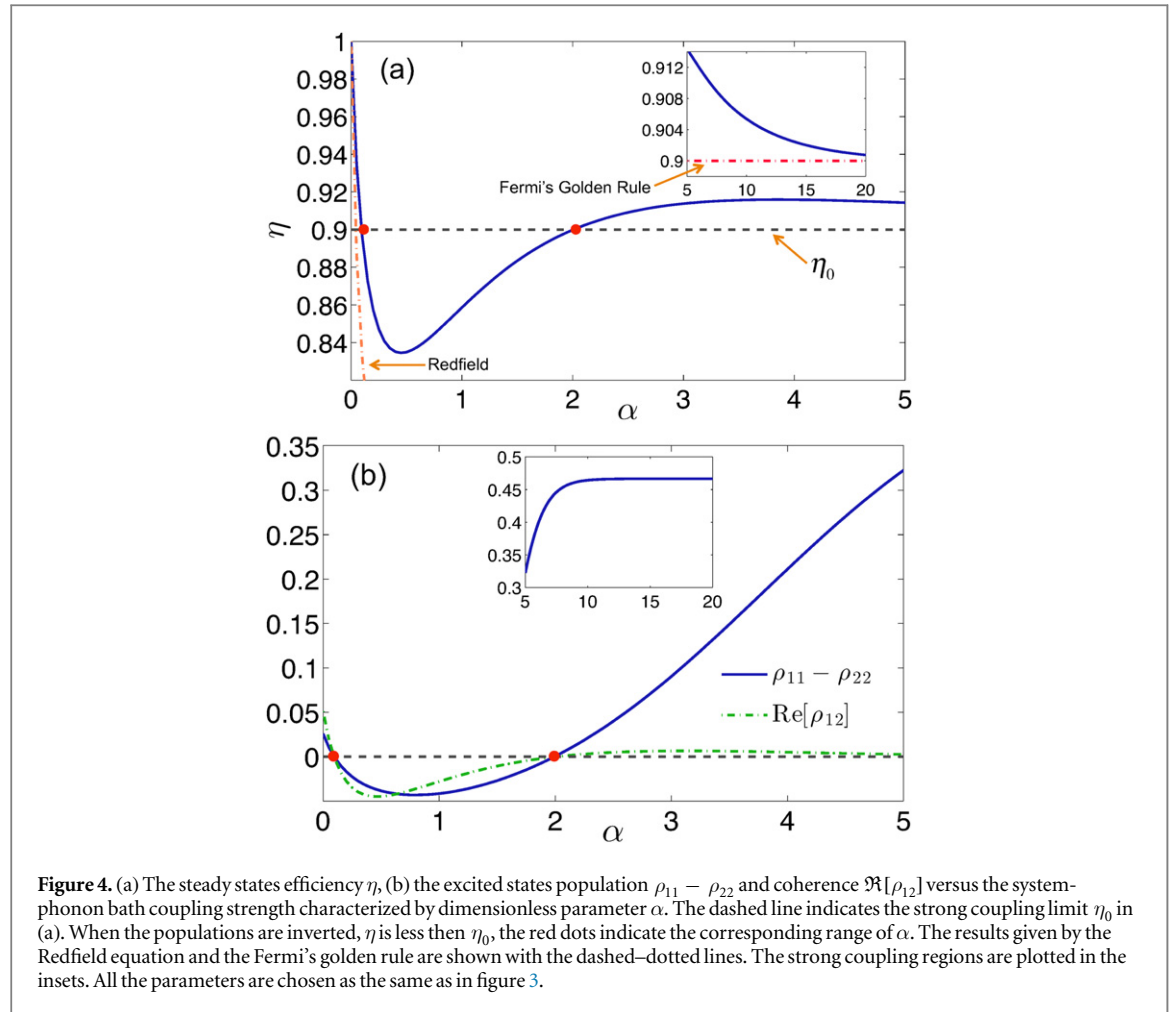
$$\gamma_p [n_p \rho_{00} - (n_p + 1) \rho_{11}] = \gamma_t [(n_t + 1) \rho_{22} - n_t \rho_{00}]. \quad (21)$$

With this relation, the efficiency in the strong coupling limit reads

$$\eta \approx -\frac{\epsilon_2 \gamma_t [(n_t + 1) \rho_{22} - n_t \rho_{00}]}{\epsilon_1 \gamma_p [(n_p + 1) \rho_{11} - n_p \rho_{00}]} = \frac{\epsilon_2}{\epsilon_1}. \quad (22)$$

This result indicates that when the coherence is negligible due to the strong system-phonon coupling, the energy transfer efficiency η approaches η_0 , which is consistent with the key result of [12]. We notice that equation (21) shows that the net rate of pumping one excitation to $|1\rangle$ equals to the net rate of trapping one excitation from $|2\rangle$ to $|0\rangle$. In general, the efficiency is closely related to the phonon bath induced coherence [33] of the excited states. If we require the system outputs positive energy, i.e., $\gamma_t (n_t + 1) \rho_{22} > \gamma_t n_t \rho_{00}$, then according to equations (19)–(21), $\Re[\rho_{12}] > 0$ leads to $\eta > \eta_0$ and vice versa.

According to our discussion of the flux in the last subsection, when the coupling strength $\alpha = 0$, the energy transfer efficiency $\eta = 1$ because there is no loss of energy flux. When the coupling strength gradually increases, the efficiency decreases. However, after reaching its minimum value, the efficiency starts to rise with α , which is shown in figure 4(a). The increase of efficiency assisted by noise was studied extensively in the context of energy transfer in light-harvesting systems [34–36]. As we further increase α , the efficiency grows beyond the strong



coupling limit η_0 and then gradually approaches this limit from above. The strong coupling region is plotted in the inset of figure 4(a).

Interestingly, we find population inversion of the two excited states in the regimes of $\eta > \eta_0$. We plot the population difference between states $|1\rangle$ and $|2\rangle$ in figure 4(b). In the intermediate coupling region indicated between the two red dots, the steady state population satisfies $\rho_{11} < \rho_{22}$ (the effective temperature associates with these two states is positive), the corresponding efficiency η is less than η_0 as shown in figure 4(a). On the contrary, outside this intermediate region, i.e., when the coupling is either very weak or very strong, the populations are inverted $\rho_{11} > \rho_{22}$ (the effective temperature is negative); meanwhile η increase beyond η_0 . In the local basis, the population and coherence are coupled with each other due to the polaron effects: the population inversion happens when $\Re[\rho_{12}] < 0$ (figure 4(b)). The fact that the population and coherence in the local basis have similar behavior can be explained from equation (A9) and equation (A10). Here, the coherence $\langle \tau_x(t) \rangle$ in the polaron basis is negligibly small (see the inset of figure C1 in appendix C) to have significant effects, then the terms $\langle \sigma_z \rangle = \rho_{11} - \rho_{22}$ and $\langle \sigma_x \rangle = 2\Re[\rho_{12}]$ are both determined by $\langle \tau_z \rangle$.

In figure 4(a), we also compare the efficiency η calculated by the PTRE method with those predicted by the Redfield equation and the Fermi's golden rule approaches. As we mentioned before, in the weak and strong coupling limits, the PTRE method agrees with the Redfield equation and the Fermi's golden rule, respectively, and it connects these two limits with a non-trivial minimum which is related to the coherence in the local basis.

4.3. Further discussions

4.3.1. Kinetic models

In the strong coupling regime, we can map this energy transfer process into a simple excitation kinetic model as shown in figure 5(a). Each step of energy transfer is described by an effective flux ($\mathcal{J}_p^{\text{eff}}$, $\mathcal{J}_v^{\text{eff}}$ and $\mathcal{J}_t^{\text{eff}}$). The relaxation of the two excited states is characterized by the rate γ_z , which is defined in equation (C2) of appendix C. As shown in figure 5(b), the effective transfer flux $\mathcal{J}_v^{\text{eff}}$ between the two excited states is approximately proportional to the relaxation rate γ_z . When $\mathcal{J}_v^{\text{eff}}$ (or γ_z) is smaller than the trapping flux $\mathcal{J}_t^{\text{eff}}$ (or γ_t), the excitation in excited states will be quickly captured by the trapping field without enough time to first get

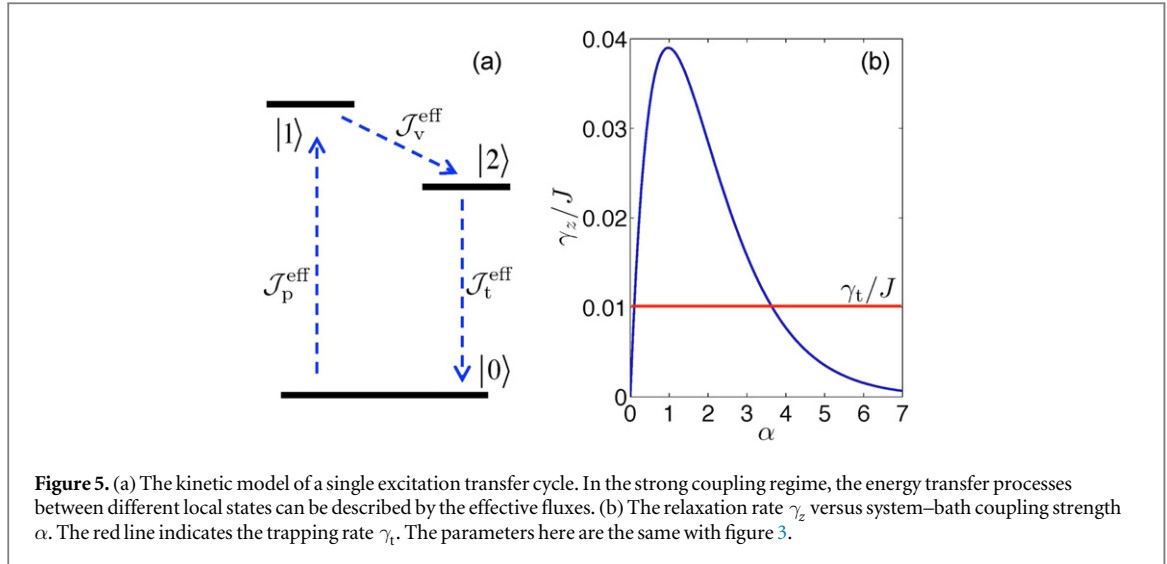


Figure 5. (a) The kinetic model of a single excitation transfer cycle. In the strong coupling regime, the energy transfer processes between different local states can be described by the effective fluxes. (b) The relaxation rate γ_z versus system–bath coupling strength α . The red line indicates the trapping rate γ_t . The parameters here are the same with figure 3.

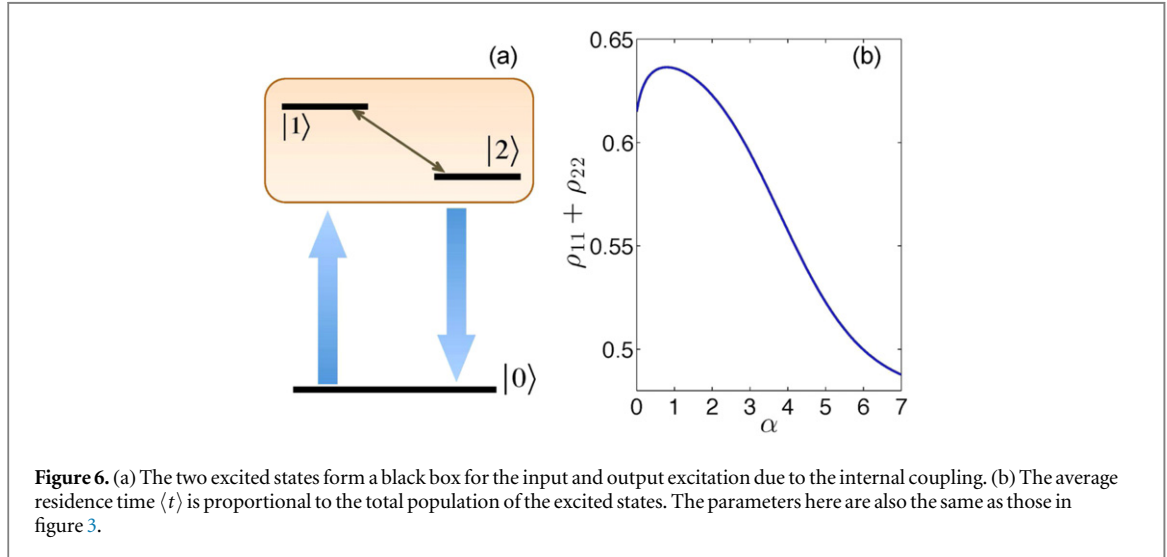


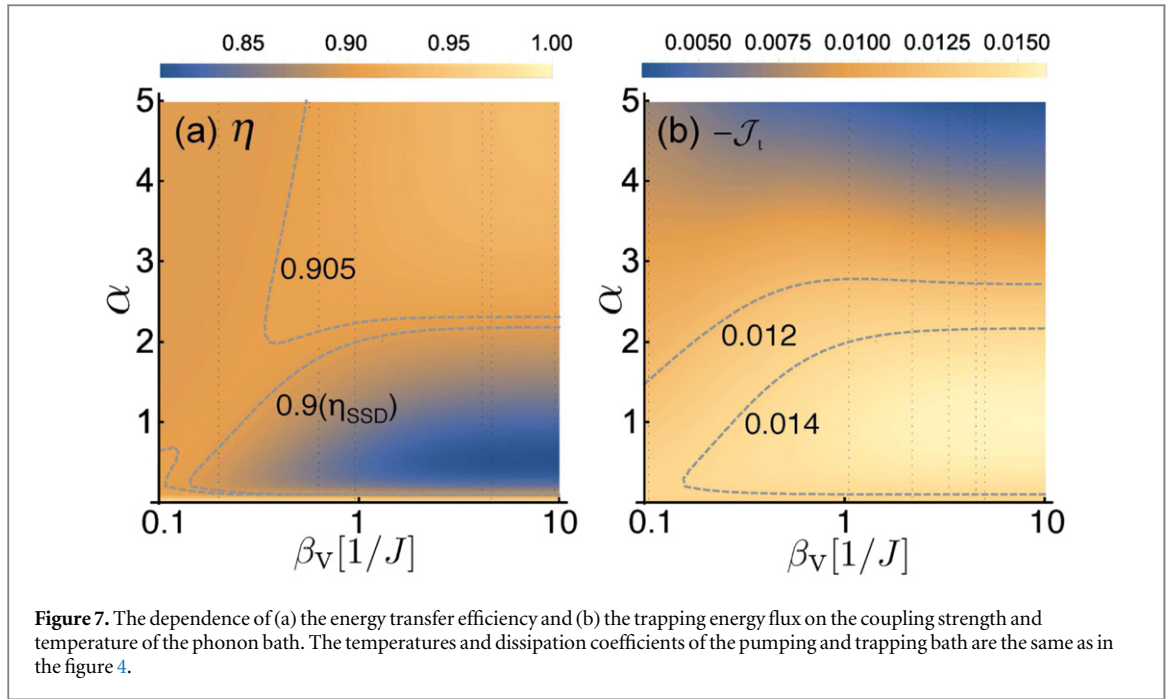
Figure 6. (a) The two excited states form a black box for the input and output excitation due to the internal coupling. (b) The average residence time $\langle t \rangle$ is proportional to the total population of the excited states. The parameters here are also the same as those in figure 3.

equilibrated with the phonon bath. Consequently, the populations of the two excited states are inverted and the real part of the coherence becomes negative. This phenomenological mechanism explains why the efficiency η is higher than η_0 in the strong coupling limit.

When the system–bath coupling strength becomes weaker, the local basis frame is no longer a good option for the kinetic picture. The two excited states couple with each other and can be together considered as an excited state manifold, as shown in figure 6(a). The single excitation carrying certain amount of energy passes through the excited states $|1\rangle$ and $|2\rangle$, and its average residence time $\langle t \rangle$ in the excited states is negatively correlated with the transfer efficiency (in analogy to the light-harvesting efficiency in [36, 37]): i.e., the longer the excitation stays in the excited states, the more energy will be lost to the phonon bath, and the lower energy transfer efficiency will be. During a cycle that the single excitation starts from $|0\rangle$ and finally returns to $|0\rangle$, the average residence time $\langle t \rangle$ is proportional to the excited states population $\rho_{11} + \rho_{22}$ at the steady states, as shown in figure 6(b). Though not quantitatively exact, this kinetic model qualitatively explains the local minimal of the efficiency η via the average residence time $\langle t \rangle \sim \rho_{11} + \rho_{22}$.

4.3.2. Temperature dependence

Besides the system–phonon bath coupling strength, the temperature of the phonon bath also affects the energy transfer process, as shown in the two-dimensional contours of energy transfer efficiency (figure 7(a)) and trapping energy flux (figure 7(b)). The efficiency behaves the same at the high phonon bath temperature as in the strong coupling. In the high temperature limit, even when the coupling strength is weak, the efficiency is still close to η_0 . As seen from equation (13), in either limit $\alpha \rightarrow \infty$ or $\beta_v \rightarrow 0$, the renormalization factor $\kappa \rightarrow 0$; therefore, except for the weak coupling and low temperature case, the efficiency η does not change obviously.



The trapping energy flux has a different temperature dependences for weak and strong system–bath couplings. The flux $-\mathcal{J}_t$ grows (goes down) with descending β_v when α is large (small). Moreover, $-\mathcal{J}_t$ does not sensitively depend on β_v with small α in contrast with the efficiency. When the coupling α is around 1, the flux $-\mathcal{J}_t$ changes no more than 20% in amplitude comparing with its maximum. The optimization of the efficiency and the trapping flux can be achieved in two different regimes: (1) The coupling strength is weak and the temperature of the phonon bath is high. (2) The coupling strength is medium ($\alpha \sim 2.5$) and the bath temperature is low ($\beta_v > 1$). The first regime corresponds to the high temperature classical limit, and the second regime corresponds to low-temperature quantum regime, where bath-induced coherence enhances the energy transfer process.

5. Conclusion

In this paper we use the PTRE to analyse the effects of the phonon bath on the energy transfer process in a generic three-level model. As a quantitative method, the PTRE can reliably describe the dependence of the steady state coherence on the system–bath coupling strength ranging from the weak to strong coupling regime. Our analysis shows that the steady state coherence between the two excited states is crucial to the energy transfer efficiency. When the effective temperature of the excited states is negative (populations are inverted), the coherence carries a positive real part and enhances the efficiency beyond the strong coupling limit η_0 . On the contrary, if the effective temperature is positive (populations are not inverted), the coherence carries a negative real part and is detrimental to the efficiency. The energy flux and efficiency compete with each other and cannot reach maximum simultaneously; however, the study of their behaviors with respect to the coupling strength and temperature provides the key information about how to make an optimal compromise between the two quantities. We will consider how to use quantum control to optimize the energy transfer process in the future study.

Acknowledgments

DX and YZ were supported by the National Research Foundation, Republic of Singapore, through the Competitive Research Program (CRP) under Project No. NRF-CRP5-2009-04. JC acknowledges the National Science Foundation (NSF) of the US (Grant No. CHE-1112825). CW has been supported by the Singapore-MIT Alliance for Research and Technology (SMART).

Appendix A. Secular-Markovian Redfield equation in the polaron frame

The two excited states coupled with the phonon bath is described by the Hamiltonian in equations (1) and (4), which is broadly studied as the spin-boson model. Via the polaron transformation given in equation (9), the system-bath coupling is effectively weakened to the order of the thermal-fluctuation, hence the second-order perturbation theory can be applied. With the secular-Markov approximation, the PTRE for spin-boson model in the interaction picture is given by

$$\frac{d\rho_s^{II}(t)}{dt} = - \int_0^\infty ds \text{Tr}_b \{ [\tilde{V}(t), [\tilde{V}(t-s), \rho_s^{II}(t) \otimes \rho_b']] \}, \quad (\text{A1})$$

which can be further written in the Schrodinger picture as equation (15)

$$\begin{aligned} \frac{d\rho_s'(t)}{dt} = & -i[\tilde{H}_0, \rho_s'(t)] - \sum_{i,j=z,\pm} [\Gamma_{ij}^+ \tau_i \tau_j \rho_s'(t) + \Gamma_{ji}^- \rho_s'(t) \tau_j \tau_i \\ & - \Gamma_{ji}^- \tau_i \rho_s'(t) \tau_j - \Gamma_{ij}^+ \tau_j \rho_s'(t) \tau_i]. \end{aligned}$$

Here, the Pauli operators τ_i defined by the eigenstates of \tilde{H}_0 are given in equations (16) and (17), and

$$|+\rangle = \cos \frac{\theta}{2} |1\rangle + \sin \frac{\theta}{2} |2\rangle, \quad (\text{A2})$$

$$|-\rangle = \sin \frac{\theta}{2} |1\rangle - \cos \frac{\theta}{2} |2\rangle, \quad (\text{A3})$$

where $\tan \theta = \kappa J / \epsilon$. The dissipation rates Γ_{ij}^\pm are related to the bath correlation functions

$$\Gamma_{ij}^\pm = \frac{\Delta_\kappa^2}{4} \int_0^\infty dt \langle \xi_i(\pm t) \xi_j(0) \rangle, \quad (\text{A4})$$

with

$$\xi_z(t) = \sin \theta [\cos B(t) - \kappa], \quad (\text{A5})$$

$$\xi_\pm(t) = -e^{\pm i \Delta_\kappa t} [\cos \theta [\cos B(t) - \kappa] \mp i \sin B(t)], \quad (\text{A6})$$

where $\Delta_\kappa = \sqrt{\epsilon^2 + (\kappa J)^2}$ and $B(t) = e^{i \tilde{H}_0 t} B e^{-i \tilde{H}_0 t}$.

To transform equation (15) back into the local frame, we express the elements of the RDM $\rho_s'(t)$ and $\rho_s(t)$ by the average of the Pauli operators $\langle \tau_{z,\pm}(t) \rangle \equiv \text{Tr}_s[\rho_s'(t) \tau_{z,\pm}]$ and $\langle \sigma_{z,\pm}(t) \rangle \equiv \text{Tr}_s[\rho_s(t) \sigma_{z,\pm}]$. As σ_z commutes with the polaron-transformation, the diagonal term $\langle \sigma_z(t) \rangle$ is easily to obtained from $\rho_s'(t)$,

$$\begin{aligned} \langle \sigma_z(t) \rangle &= \text{Tr}_{s+b}[\rho_{\text{tot}}(t) \sigma_z] = \text{Tr}_s[\rho_s(t) \sigma_z] \\ &= \text{Tr}_{s+b}[\rho_{\text{tot}}'(t) \sigma_z] = \text{Tr}_s[\rho_s'(t) \sigma_z], \end{aligned} \quad (\text{A7})$$

where $\rho_{\text{tot}}(t)$ is the total density matrix for the TLS and its bath, $\rho_s(t) = \text{Tr}_b[\rho_{\text{tot}}(t)]$ and $\rho_{\text{tot}}'(t) = e^{-i \sigma_z B / 2} \rho_{\text{tot}}(t) e^{i \sigma_z B / 2}$ is the polaron-transformed total density matrix. However, the polaron transformation operator and σ_x (σ_y) do not commute, thus the off-diagonal terms cannot be obtained exactly. This problem can be solved by using the Born approximation $\rho_{\text{tot}}'(t) \approx \rho_s'(t) \otimes \rho_b'$, which has already been used in deriving the PTRE. The polaron transformation reduces the system-bath coupling, thus makes the factorization of the density matrix in the polaron frame reasonable. Therefore, we have

$$\langle \sigma_{x,y}(t) \rangle = \text{Tr}_{s+b}[\rho_{\text{tot}}'(t) e^{-i \sigma_z B / 2} \sigma_{x,y} e^{i \sigma_z B / 2}] \approx \kappa \text{Tr}_s[\rho_s'(t) \sigma_{x,y}]. \quad (\text{A8})$$

Together with equations (A2) and (A3), it is straightforwardly to obtain

$$\langle \sigma_z(t) \rangle = \cos \theta \langle \tau_z(t) \rangle + \sin \theta \langle \tau_x(t) \rangle, \quad (\text{A9})$$

$$\langle \sigma_x(t) \rangle = \kappa \sin \theta \langle \tau_z(t) \rangle - \kappa \cos \theta \langle \tau_x(t) \rangle, \quad (\text{A10})$$

$$\langle \sigma_y(t) \rangle = -\kappa \langle \tau_y(t) \rangle \quad (\text{A11})$$

following which the expression for the Liouville operator \mathcal{L}_v of the TLS is derived.

Appendix B. Weak and strong coupling limits of PTRE

In this appendix, we would like to show that the PTRE in the weak (strong) coupling limit is exactly consistence with the Redfield equation (rate equation based on the Fermi's golden rule). In the weak coupling limit, we have $\kappa \approx 1$, thus the polaron basis $|\pm(\Delta_\kappa)\rangle$ approaches the eigenbasis of the TLS $|\pm(\Delta_0)\rangle$, where $\Delta_0 = \sqrt{\epsilon^2 + J^2}$. In this eigen frame, the PTRE equation (15) with secular approximation is reduced to the Redfield equation

$$\frac{d}{dt}[\rho_s]_{++} = -\Gamma[1 + n(\Delta_0)][\rho_s]_{++} + \Gamma n(\Delta_0)[\rho_s]_{--}, \quad (\text{B1})$$

$$\frac{d}{dt}[\rho_s]_{+-} = -\left[i\Delta + \frac{1}{2}\Gamma(1 + 2n(\Delta_0))\right][\rho_s]_{+-}, \quad (\text{B2})$$

where $\Gamma = \frac{1}{2}J(\Delta_0)\sin^2\theta$.

In the strong coupling limit, the coherence is quickly destroyed by dissipation, thus we only need to consider the equations for the populations. Additionally, as $\kappa \approx 0$ with large α , the eigenbasis of \tilde{H}_0 are reduced to the local basis $|1\rangle$ and $|2\rangle$. As a result, equation (15) becomes a kinetic equation governing the populations $P_i \equiv [\rho_s]_{ii}$, which can be written as

$$\frac{d}{dt}P_1 = -\Gamma_{12}P_1 + \Gamma_{21}P_2, \quad (\text{B3})$$

where

$$\Gamma_{12} = \frac{1}{2}\kappa^2 J^2 \int_0^\infty d\tau \Re[e^{i\epsilon\tau}(e^{Q(\tau)} - 1)], \quad (\text{B4})$$

$$\Gamma_{21} = \frac{1}{2}\kappa^2 J^2 \int_0^\infty d\tau \Re[e^{-i\epsilon\tau}(e^{Q(\tau)} - 1)], \quad (\text{B5})$$

with

$$Q(\tau) = \int_0^\infty d\omega \frac{J(\omega)}{\pi\omega^2} [\cos(\omega\tau) \coth(\beta_v\omega/2) - i \sin(\omega\tau)]. \quad (\text{B6})$$

The above transition rates Γ_{12} and Γ_{21} are the same as those obtained from the Fermi's golden rule. In a word, the PTRE smoothly connects the weak and strong coupling limits, and provides a useful tool to study the intermediate coupling region where there is usually no reliable approximation methods.

Furthermore, following from equation (B3) the three-level system in the strong coupling limit can be understood from the perspective of population kinetics. The population transitions rate from state $|i\rangle$ to $|j\rangle$ is denoted by Γ_{ij} , then the net population flux from $|i\rangle$ to $|j\rangle$ is $\Gamma_{ij}P_i - \Gamma_{ji}P_j$. In the steady state, the net population fluxes between each two local states must be equal with each other due to population conservation, which means there is a circulation F in the three-level system:

$$F = \Gamma_{12}P_1 - \Gamma_{21}P_2 = \Gamma_{20}P_2 - \Gamma_{02}P_0 = \Gamma_{01}P_0 - \Gamma_{10}P_1. \quad (\text{B7})$$

Then the energy flux from $|i\rangle$ to $|j\rangle$ is just the population flux F times the corresponding energy gap, $\mathcal{J}_{i \rightarrow j} = F(\epsilon_i - \epsilon_j)$, which directly leads to the efficiency $\eta_0 = \epsilon_2/\epsilon_1$. With straightforward calculation, we obtain the steady state population $P_i = D_i/D$ from the kinetic equation (B7), where

$$D_1 = \Gamma_{01}\Gamma_{20} + \Gamma_{02}\Gamma_{21} + \Gamma_{21}\Gamma_{01}, \quad (\text{B8})$$

$$D_2 = \Gamma_{02}\Gamma_{10} + \Gamma_{01}\Gamma_{12} + \Gamma_{12}\Gamma_{02}, \quad (\text{B9})$$

$$D_0 = \Gamma_{10}\Gamma_{20} + \Gamma_{20}\Gamma_{12} + \Gamma_{21}\Gamma_{10}, \quad (\text{B10})$$

$$D = D_1 + D_2 + D_0. \quad (\text{B11})$$

In the case of low temperature trapping bath, the transition rate Γ_{02} can be neglected comparing with Γ_{20} . Then we have $D_1 \approx \Gamma_{01}(\Gamma_{20} + \Gamma_{21})$ and $D_2 \approx \Gamma_{01}\Gamma_{12}$, then the population inversion $P_1 > P_2$ requires $\Gamma_{20} + \Gamma_{21} - \Gamma_{12} > 0$. In the strong coupling limit, the transition rates between the two excited states are almost the same $\Gamma_{12} \approx \Gamma_{21}$, thus $P_1 - P_2 \approx \Gamma_{01}\Gamma_{20}/D > 0$ is established, which is consistent with the results obtained from the PTRE.

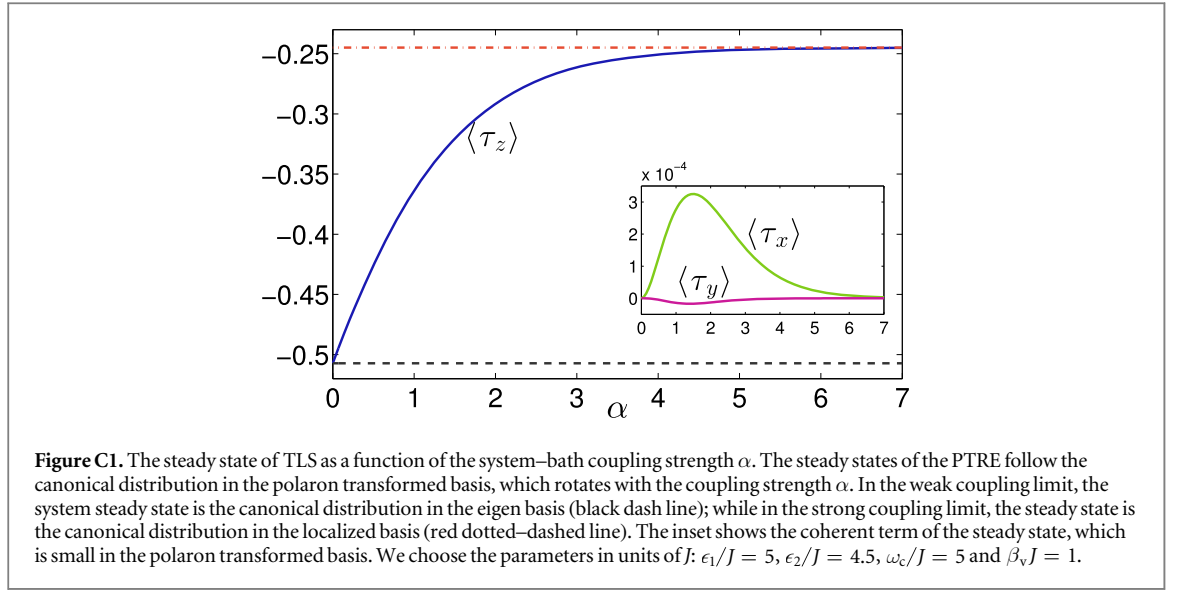
Appendix C. Steady state of the TLS in polaron frame

For convenience, we rewrite equation (15) in the form of the Bloch equation

$$\frac{d}{dt}\langle \vec{\tau}(t) \rangle = -M\langle \vec{\tau}(t) \rangle + \vec{C}. \quad (\text{C1})$$

Here $\langle \vec{\tau}(t) \rangle^T = [\langle \tau_z(t) \rangle, \langle \tau_x(t) \rangle, \langle \tau_y(t) \rangle]$. The transition matrix M and the constant term $\vec{C}^T = (C_z, C_x, C_y)$ are

$$M = \begin{pmatrix} \gamma_z & \gamma_{zx} & 0 \\ \gamma_{xz} & \gamma_x & \Delta_\kappa + \gamma_{xy} \\ \gamma_{yz} & -\Delta_\kappa + \gamma_{yx} & \gamma_y \end{pmatrix}, \quad (\text{C2})$$



$$\vec{C}^T = (C_z, C_x, C_y), \quad (\text{C3})$$

the expressions of the matrix elements are given in appendix D.

The time evolution of $\langle \vec{\tau}(t) \rangle$ is straightforwardly given by

$$\langle \vec{\tau}(t) \rangle = e^{-Mt} [\langle \vec{\tau}(0) \rangle - M^{-1}\vec{C}] + M^{-1}\vec{C}, \quad (\text{C4})$$

with the steady state $\langle \vec{\tau}(\infty) \rangle = M^{-1}\vec{C}$. In the following we will neglect time argument ∞ when referring to the steady state for convenience. The population difference $\langle \tau_z \rangle$ varies with the coupling strength as shown in figure C1. In the weak coupling limit, the TLS steady state distribution is canonical in the eigenbasis, i.e.,

$$\lim_{\alpha \rightarrow 0} \langle \tau_z \rangle = -\tanh\left(\frac{1}{2}\beta_v \Delta_0\right), \quad (\text{C5})$$

which is just the thermodynamic equilibrium state. When the system–bath coupling gradually increases, the system distribution deviates from ρ_e^{can} and follows the Boltzmann distribution

$$\langle \tau_z \rangle = -\tanh\left(\frac{1}{2}\beta_v \Delta_\kappa\right), \quad (\text{C6})$$

with respect to the energy gap Δ_κ between the eigenvalues of $|+\rangle$ and $|-\rangle$ in the polaron frame. Furthermore, when goes into the strong coupling limit, we have

$$\lim_{\alpha \rightarrow \infty} \langle \tau_z \rangle = -\tanh\left(\frac{1}{2}\beta_v \epsilon\right), \quad (\text{C7})$$

which is the Boltzmann distribution with respect to the local site energies ϵ_1 and ϵ_2 . The deviation from the canonical state ρ_s^{can} due to the strong system–bath coupling has been studied via the cumulant expansion method in the polaron-transformed thermodynamic distribution [20, 21] and from the view point of energy shell deformation [18, 19, 22].

Appendix D. Elements of the matrixes M and \vec{M}

The quantities defined in equations (C2) and (C3) are determined by the superposition of the correlation functions equation (A4) following from equations (15) and (C1). By defining the functions

$$f(t) = \cosh[Q(t)] + \cosh[Q(-t)] - 2, \quad (\text{D1})$$

$$g(t) = \sinh[Q(t)] + \sinh[Q(-t)], \quad (\text{D2})$$

it is straightforwardly to obtain

$$\gamma_z = \frac{1}{2}\kappa^2 J^2 \int_0^\infty dt \cos(\Delta_\kappa t) [f(t) \cos^2 \theta + g(t)], \quad (\text{D3})$$

$$\gamma_x = \frac{1}{2}\kappa^2 J^2 \int_0^\infty dt [f(t) \sin^2 \theta + \cos(\Delta_\kappa t) g(t)], \quad (\text{D4})$$

$$\gamma_y = \frac{1}{2}\kappa^2 J^2 \int_0^\infty dt f(t) [\cos^2 \theta \cos(\Delta_\kappa t) + \sin^2 \theta], \quad (D5)$$

$$\gamma_{zx} = \frac{1}{4}\kappa^2 J^2 \sin 2\theta \int_0^\infty dt f(t), \quad (D6)$$

$$\gamma_{xz} = \frac{1}{4}\kappa^2 J^2 \sin 2\theta \int_0^\infty dt f(t) \cos(\Delta_\kappa t), \quad (D7)$$

$$\gamma_{xy} = \frac{1}{2}\kappa^2 J^2 \int_0^\infty dt g(t) \sin(\Delta_\kappa t), \quad (D8)$$

$$\gamma_{yx} = -\frac{1}{2}\kappa^2 J^2 \cos^2 \theta \int_0^\infty dt f(t) \sin(\Delta_\kappa t), \quad (D9)$$

$$\gamma_{yz} = \frac{1}{4}\kappa^2 J^2 \sin 2\theta \int_0^\infty dt f(t) \sin(\Delta_\kappa t), \quad (D10)$$

$$C_z = -\frac{i}{2}\kappa^2 J^2 \int_{-\infty}^\infty dt \sin(\Delta_\kappa t) \times [\cos^2 \theta \cosh[Q(t)] + \sinh[Q(t)]], \quad (D11)$$

$$C_x = -\frac{i}{4}\kappa^2 J^2 \sin 2\theta \int_{-\infty}^\infty dt \sin(\Delta_\kappa t) \cosh[Q(t)], \quad (D12)$$

$$C_y = -\frac{i}{4}\kappa^2 J^2 \sin 2\theta \int_0^\infty dt [1 - \cos(\Delta_\kappa t)] \times [\cosh[Q(t)] - \cosh[Q(-t)]]. \quad (D13)$$

The Liouville operator \mathcal{L}_v for the three-level system is obtained from equation (C1) with the expressions given above. Here the relation $\rho_{00} + \rho_{11} + \rho_{22} = 1$ for the three-level system should be used to substitute $[\rho_s]_{11} + [\rho_s]_{22} = 1$ for the TLS. Taking the contributions of the Lindblad terms \mathcal{L}_p and \mathcal{L}_t defined in equation (8) into consideration, the elements of the matrix \bar{M} in equation (18) are

$$\begin{aligned} \bar{M}_{11} = & \gamma_z \cos^2 \theta + \gamma_x \sin^2 \theta + \frac{1}{2}(\gamma_{xz} + \gamma_{zx}) \sin 2\theta \\ & + \frac{1}{2}[\gamma_p(n_p + 1) + \gamma_t(n_t + 1)], \end{aligned} \quad (D14)$$

$$\bar{M}_{12} = -C_z \cos \theta - C_x \sin \theta + \frac{1}{2}[\gamma_p(3n_p + 1) - \gamma_t(3n_t + 1)], \quad (D15)$$

$$\bar{M}_{13} = \kappa^{-1} \left[\gamma_{xz} \sin^2 \theta - \gamma_{zx} \cos^2 \theta + \frac{1}{2}(\gamma_z - \gamma_x) \sin 2\theta \right], \quad (D16)$$

$$\bar{M}_{14} = -\kappa^{-1}(\Delta_\kappa + \gamma_{xy}) \sin \theta, \quad (D17)$$

$$\bar{M}_{21} = \frac{1}{2}[\gamma_p(n_p + 1) - \gamma_t(n_t + 1)], \quad (D18)$$

$$\bar{M}_{22} = \frac{1}{2}[\gamma_p(3n_p + 1) + \gamma_t(3n_t + 1)], \quad (D19)$$

$$\bar{M}_{23} = \bar{M}_{24} = 0, \quad (D20)$$

$$\bar{M}_{31} = \kappa \left[\gamma_{zx} \sin^2 \theta - \gamma_{xz} \cos^2 \theta + \frac{1}{2}(\gamma_z - \gamma_x) \sin 2\theta \right], \quad (D21)$$

$$\bar{M}_{32} = \kappa(C_x \cos \theta - C_z \sin \theta), \quad (D22)$$

$$\begin{aligned} \bar{M}_{33} = & \gamma_x \cos^2 \theta + \gamma_z \sin^2 \theta - \frac{1}{2}(\gamma_{xz} + \gamma_{zx}) \sin 2\theta \\ & + \frac{1}{2}[\gamma_p(n_p + 1) + \gamma_t(n_t + 1)], \end{aligned} \quad (D23)$$

$$\bar{M}_{34} = (\Delta_\kappa + \gamma_{xy}) \cos \theta, \quad (D24)$$

$$\bar{M}_{41} = \kappa[(\Delta_\kappa - \gamma_{yx}) \sin \theta - \gamma_{yz} \cos \theta], \quad (D25)$$

$$\bar{M}_{42} = \kappa C_y, \quad (D26)$$

$$\bar{M}_{43} = -(\Delta_\kappa \gamma_{yx}) \cos \theta - \gamma_{yz} \sin \theta, \quad (D27)$$

$$\bar{M}_{44} = \gamma_y + \frac{1}{2}[\gamma_p(n_p + 1) + \gamma_t(n_t + 1)]. \quad (D28)$$

References

- [1] Engel G S, Calhoun T R, Read E L, Ahn T-K, Mancal T, Cheng Y-C, Blankenship R E and Fleming G R 2007 *Nature* **446** 782
- [2] Ishizaki A and Fleming G R 2009 *Proc. Natl Acad. Sci.* **106** 7255
- [3] Cao J and Silbey R J 2009 *J. Phys. Chem. A* **113** 13826
- [4] Tscherbul T V and Brumer P 2014 *Phys. Rev. Lett.* **113** 113601
- [5] Olšna J, Dijkstra A G, Wang C and Cao J 2014 arXiv:1408.5385
- [6] Quan H T, Liu Y X, Sun C P and Nori F 2007 *Phys. Rev. E* **76** 031105
- [7] Scully M O, Chapin K R, Dorfman K E, Kim M B and Svidzinsky A 2011 *Proc. Natl Acad. Sci.* **108** 15097
- [8] Dorfman K E, Voronine D V, Mukamel S and Scully M O 2011 *Proc. Natl Acad. Sci.* **110** 2746
- [9] Scovil H E D and Schulz-DuBois E O 1959 *Phys. Rev. Lett.* **2** 262
- [10] Geusic J E, Schulz-DuBois E O and Scovil H E 1967 *Phys. Rev.* **156** 343
- [11] Geva E and Kosloff R 1996 *J. Chem. Phys.* **104** 7681
- [12] Boukobza E and Tannor D J 2006 *Phys. Rev. A* **74** 063823
- [13] Boukobza E and Tannor D J 2007 *Phys. Rev. Lett.* **98** 240601
- [14] Linden N, Popescu S and Skrzypczyk P 2010 *Phys. Rev. Lett.* **105** 130401
- [15] Levy A and Kosloff R 2012 *Phys. Rev. Lett.* **108** 070604
- [16] Rahav S, Harbola U and Mukamel S 2012 *Phys. Rev. A* **86** 043843
- [17] Correa L A, Palao J P, Alonso D and Adesso G 2014 *Sci. Rep.* **4** 3949
- [18] Dong H, Yang S, Liu X F and Sun C P 2007 *Phys. Rev. A* **76** 044104
- [19] Dong H, Liu X F and Sun C P 2010 *Chin. Sci. Bull.* **55** 3256
- [20] Lee C K, Cao J and Gong J B 2012 *Phys. Rev. E* **86** 021109
- [21] Lee C K, Moix J and Cao J 2012 *J. Chem. Phys.* **136** 204120
- [22] Xu D Z, Li S W, Liu X F and Sun C P 2014 *Phys. Rev. E* **90** 062125
- [23] Grover M and Silbey R J 1971 *J. Chem. Phys.* **54** 4843
- [24] Silbey R J and Harris T 1984 *J. Chem. Phys.* **80** 2615
- [25] Wang C, Ren J and Cao J 2015 *Sci. Rep.* **5** 11787
- [26] Wang C, Ren J and Cao J 2014 *New J. Phys.* **16** 045019
- [27] Zimanyi E N and Silbey R J 2012 *Phil. Trans. R. Soc. A* **370** 3620
- [28] Lee C K, Moix J M and Cao J 2015 *J. Chem. Phys.* **142** 164103
- [29] McCutcheon D A P S and Nazir A 2011 *J. Chem. Phys.* **135** 114501
- [30] Curzon F and Ahlborn B 1975 *Am. J. Phys.* **43** 22
- [31] Van den Broeck C 2005 *Phys. Rev. Lett.* **95** 190602
- [32] Esposito M, Lindenberg K and Van den Broeck C 2009 *Phys. Rev. Lett.* **102** 130602
- [33] Dijkstra A G, Wang C, Cao J and Fleming G R 2015 *J. Phys. Chem. Lett.* **6** 627
- [34] Caruso F, Chin A W, Datta A, Huelga S F and Plenio M B 2009 *J. Chem. Phys.* **131** 105106
- [35] Rebentrost P, Mohseni M, Kassal I, Lloyd S and Aspuru-Guzik A 2009 *New J. Phys.* **11** 033003
- [36] Wu J L, Liu F, Shen Y, Cao J and Silbey R J 2010 *New J. Phys.* **12** 105012
- [37] Wu J, Silbey R J and Cao J 2013 *Phys. Rev. Lett.* **110** 200402